

**Topological Characterization and Global Vector Field
Reconstruction of an Experimental Electrochemical System**

C. Letellier, L. Le Sceller, P. Dutertre, G. Gouesbet, Z. Fei, and J. L. Hudson

J. Phys. Chem., **1995**, 99 (18), 7016-7027 • DOI: 10.1021/j100018a039 • Publication Date (Web): 01 May 2002

Downloaded from <http://pubs.acs.org> on March 9, 2009

More About This Article

The permalink <http://dx.doi.org/10.1021/j100018a039> provides access to:

- Links to articles and content related to this article
- Copyright permission to reproduce figures and/or text from this article



ACS Publications
High quality. High impact.

Topological Characterization and Global Vector Field Reconstruction of an Experimental Electrochemical System

C. Letellier, L. Le Sceller, P. Dutertre, and G. Gouesbet

Laboratoire d'Énergétique des Systèmes et Procédés, URA CNRS 230, INSA de Rouen, BP 08, 76 130 Mont-Saint-Aignan, France

Z. Fei and J. L. Hudson*

Department of Chemical Engineering, University of Virginia, Charlottesville, Virginia 22903

Received: November 2, 1994[®]

A complete study of a copper electrodisolution experiment is achieved. The asymptotic motion settles down on a strange chaotic attractor which may be embedded in a 3D reconstructed space. In a 2D Poincaré section the attractor is found to be topologically equivalent to a 1D map, and its orbit spectrum is governed by the unimodal order. A set of equations which suitably model the experiment is extracted by a global vector field reconstruction method. The attractor obtained by integrating the reconstructed system is topologically equivalent to the original attractor. It is shown that the reconstructed model represents the dynamics without taking into account the effect of the dynamical noise on the experiment.

I. Introduction

Periodic and chaotic oscillations have been observed in a number of electrochemically reacting systems.¹ Experiments are normally conducted potentiostatically, in which case the current oscillates, or galvanostatically, where the oscillations are in the potential. We are interested in the characterization of time series from such reactions and the development of mathematical models in order to increase the understanding of the dynamic behavior and its dependence on parameters. However, it is often the case that such models do not exist, or they may not be able to be used to extract the dynamics. In such cases, ad hoc models developed directly from the experimental data can sometimes be used to characterize and predict the system dynamics. One such approach which has been used to characterize time series from chemical reaction processes is artificial neural networks (ANN).²⁻⁵ ANNs have been able to reproduce chaotic attractors and a bifurcation sequence of period doublings to chaos. Of particular relevance to the present paper is the work of Rico-Martínez et al.⁴ in which a global vector field reconstruction was obtained using continuous-time modeling with artificial neural networks. In this paper we develop another vector field reconstruction of chemical chaos in the same electrochemical system, and we show that additional information about the structure of the dynamics can be obtained. The reaction considered is the electrodisolution of copper in phosphoric acid. It has been known for some time that oscillations can occur in this system,⁶ and the reaction has received considerable attention since that time; see, for example, refs 7 and 8. An extensive study of the dynamics of the reaction has been carried out by Schell and co-workers,^{9,10} who showed the existence of Farey sequences of mixed-mode oscillations, period doublings to chaos, alternating periodic and chaotic states, etc.

II. Theoretical Background

A. Reconstruction Method. In the last few years, many papers have been devoted to global vector field recon-

struction.¹¹⁻²³ In particular, the extraction of a set of equations which models the experimental data is a very important goal in the study of nonlinear systems. If a good equivalence between the original attractor and the reconstructed attractor is achieved (for helpful discussion about this problem, see ref 24), information on the evolution of the unobserved coupled variables required for the complete description of the system may then be available.

Let us consider a nonlinear dynamical system defined by a set of autonomous ordinary differential equations:

$$\dot{\mathbf{x}} = \mathbf{f}(\mathbf{x}; \boldsymbol{\mu}) \quad (1)$$

in which $\mathbf{x}(t) \in \mathbb{R}^n$ is a vector-valued function depending on a parameter t called the time and \mathbf{f} , the so-called vector field, is an n -component smooth function generating a flow ϕ_t . $\boldsymbol{\mu} \in \mathbb{R}^p$ is the parameter vector with p components, assumed to be constant in this paper. The system (1) is called the original system and is unknown in the experimental cases. Without any loss of generality, we present the method with $n = 3$. The original system may therefore be written as

$$\begin{aligned} \dot{x} &= f_1(x, y, z) \\ \dot{y} &= f_2(x, y, z) \\ \dot{z} &= f_3(x, y, z) \end{aligned} \quad (2)$$

From an experimental point of view, only one variable is recorded as a scalar time series. Let us take it to be x .

The aim is thereafter to reconstruct a vector field equivalent to the original system under the form of a standard system made of the observable and of its derivative according to

$$\begin{aligned} \dot{X} &= \dot{x} = Y \\ \dot{Y} &= Z \\ \dot{Z} &= F_s(X, Y, Z) \end{aligned} \quad (3)$$

in which the reconstructed state space related to the standard system is spanned by derivatives coordinates (X, Y, Z) with $X = x$.

[®] Abstract published in *Advance ACS Abstracts*, April 15, 1995.

A global vector field reconstruction may then be achieved if a good enough approximation \tilde{F}_s of the so-called standard function F_s is designed. The approximation \tilde{F}_s is obtained by using a Fourier expansion on a basis of orthonormal multivariate polynomials generated on the data set.¹⁷⁻²³ These polynomials depend on the derivative coordinates (X, Y, Z) , therefore involving terms reading $(X^i Y^j Z^k)$. As described in ref 23, we introduce monomials P^l which read

$$P^l = X^i Y^j Z^k \quad (4)$$

The one-to-one relationship between triplets (i, j, k) and natural numbers l is completely defined in ref 23. The approximation of the function may then be written as follows:

$$\tilde{F}_s = \sum_{l=1}^{N_l} K_l P^l \quad (5)$$

where N_l is the dimension of the basis $\{P^l\}$. All the information concerning the chaotic attractor is therefore encoded in the set of coefficients K_l , which forms a signature of the attractor.

The time derivatives used in this algorithm are estimated by a discrete linear filter

$$w_j(t) = \sum_{n=-p}^p r_{j,p}(n)x(t+n\tau) \quad (6)$$

where the time series $x(t)$ discretized on the time step τ is the input, $w_j(t)$, the so-called Legendre coordinate, the output, and $r_{j,p}(n)$ is an appropriate discrete convolution kernel, namely the discrete Legendre polynomials, parametrized by the choice of p and the order j of the desired derivative.²⁵

After an expansion in a Taylor series, we obtain

$$w_j(t) = \sum_{i=0}^{\infty} \frac{\tau^i}{i!} x^{(i)}(t) \left[\sum_{n=-p}^p n^i r_{j,p}(n) \right] \quad (7)$$

where $r_{j,p}$ are the discrete Legendre polynomials given in ref 25. After algebraic manipulations, the following relation is obtained:

$$w_j(t) = \frac{c_j(p)\tau_w^j}{2^j j!} x^{(j)}(t) + \mathcal{O}(\tau_w^{j+2}) \quad (8)$$

where c_j is a normalization constant and $\tau_w = (2p+1)\tau$ is the window size. The Legendre coordinates are then proportional to the j th-order derivative $x^{(j)}(t)$ with a constant of proportionality determined by j , p , and τ_w . Following Gibson *et al.*,²⁵ this filter defines the optimal linear coordinate transformation.

It is then found²³ that the reconstruction depends on N_q , the number of points $(X_i, Y_i, Z_i, \dot{Z}_i)$ ($i \in [1, N_q]$) on the net, N_s , the number of net points sampled per pseudoperiod, N_p , the number of retained multivariate polynomials, and τ_w , the window size on which are estimated the derivatives by using the linear filter (6). The vector $(\tau, N_q, N_s, N_p, \tau_w)$ is called the driving vector and defines all the reconstruction parameters. In practical applications, the choice of such parameters may have a significant effect on the quality of the results.²³ A guideline for choosing a generally good driving vector is based on an error function E_r according to

$$E_r = \frac{\sum_{i=1}^{N_q} |\dot{Z}_i - \tilde{F}_s(X_i, Y_i, Z_i)|}{\sum_{i=1}^{N_q} |\dot{Z}_i|} \quad (9)$$

This error function is calculated by using absolute values for computational efficiency.

E_r may be understood as a relative error between the value of the standard function directly evaluated from the time series and the one obtained from its approximation. For a given value of N_q , optimal values for N_s and the number of polynomials N_p are obtained by minimizing the error function. However, the value of N_q at which the minimized error function passes through a minimum or a local minimum does not warrant a correct integration. Therefore, the search of a successful global vector field reconstruction needs systematical trials, which are possible with computational help. The use of such an error function is similar to the one of the least-squares minimization term proposed by Brown *et al.*²⁶ and is very convenient for the global vector field reconstruction method here developed.

B. Topological Characterization. In the last few years, several works discussed the topological description of chaotic attractors. In particular, the idea has arisen that an attractor can be described by the population of periodic orbits, their related symbolic dynamics, and their linking numbers.²⁷ In three-dimensional cases, periodic orbits may be viewed as knots,²⁸ and consequently, they are robust with respect to smooth parameter changes and allow the definition of topological invariants under isotropy (continuous deformation).

The topological approach is based on the organization of periodic orbits. We now present the basic concepts of topological characterization and symbolic dynamics. For the sake of simplicity, we use the well-known Rössler attractor as an example.

1. *Template.* The Rössler system²⁹ reads

$$\begin{aligned} \dot{x} &= -y - z \\ \dot{y} &= x + ay \\ \dot{z} &= b + z(x - c) \end{aligned} \quad (10)$$

where (a, b, c) are the control parameters. When $(a, b, c) = (0.398, 2, 4)$, the asymptotic motion settles down on a strange chaotic attractor (Figure 1).

The attractor may be viewed as a simply stretched and folded band. Two different stripes may be exhibited from this attractor (Figure 2): one, located in the center of the attractor, is a very simple stripe without any π twist (Figure 2a); the second stripe presents a negative π twist (Figure 2b) and is therefore similar to a Möbius band.

In this way, we distinguish two topological regions on the attractor. Following a pioneering paper by Birman and Williams,³⁰ it has been shown^{27,28,31} that a template which encodes the topological properties may be built. Such a template is a convenient view of the attractor to exhibit the different stripes within the attractor and their relative organization. From the Rössler attractor, a template constituted by two stripes is extracted and displayed in Figure 3a. The band is split into two stripes, one without any π twist and one with a negative π twist (Figure 3a). Due to a standard insertion convention,³¹ stripes may be reinjected in the band from back to front and

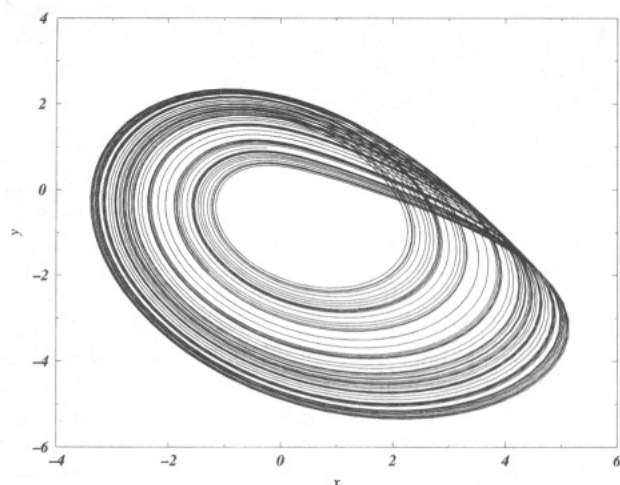


Figure 1. Rössler attractor $(a,b,c) = (0.398,2,4)$.

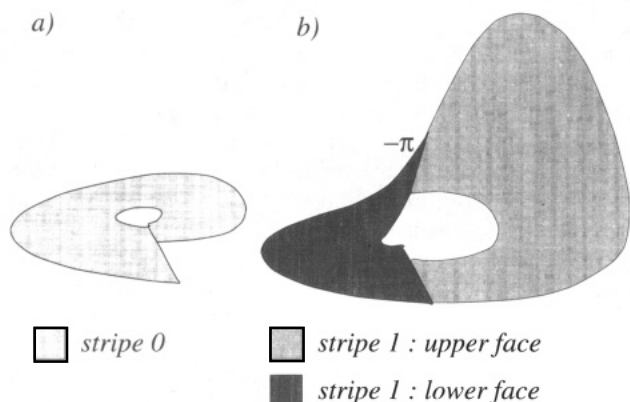


Figure 2. Two stripes of the Rössler attractor.

from left to right. Consequently, a permutation between the stripes is required, thereby leading to the configuration in Figure 3b.

This convention allows us a description of the template by a linking matrix³¹ as follows: diagonal elements $M(i,i)$ represent the π -twist number of the i th stripe and off-diagonal elements $M(i,j)$ ($i \neq j$) are given by the intersection between the i th and the j th stripe. One may check that the Rössler template is then defined by the linking matrix:

$$M \equiv \begin{pmatrix} 0 & -1 \\ -1 & -1 \end{pmatrix} \quad (11)$$

Each stripe may be labeled: symbol 0 designs the simple stripe while symbol 1 is associated with the stripe which presents a negative π twist. In this way, trajectories are encoded by a string of "0" and "1". Periodic orbits may then be encoded in a one-to-one way. We have here defined symbolic dynamics. This procedure needs a precise partition of the attractor which is given by a first-return map to a Poincaré section.

2. *First-Return Map.* A Poincaré section is here defined as the set of intersections of a chaotic trajectory with a plane transverse to the flow. For the Rössler system, such a Poincaré section is suitably defined as

$$P \equiv \{(y,z) \in \mathbb{R}^2 | x = x_-, \dot{x} > 0\} \quad (12)$$

where $x_- = (c - \sqrt{c^2 - 4ab})/2$ is the x coordinate of the central fixed point.³²

The first-return map is then computed with the y variable and displayed in Figure 4. It presents two monotonic branches: an increasing branch associated with stripe 0 and a

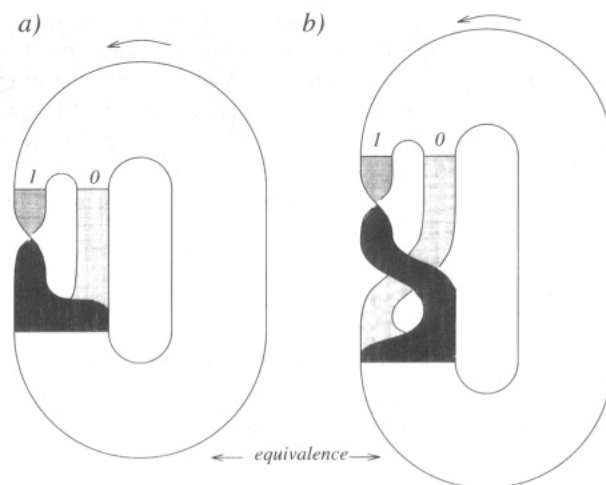


Figure 3. Template of the Rössler attractor. A permutation between the stripes is required by the standard insertion convention.

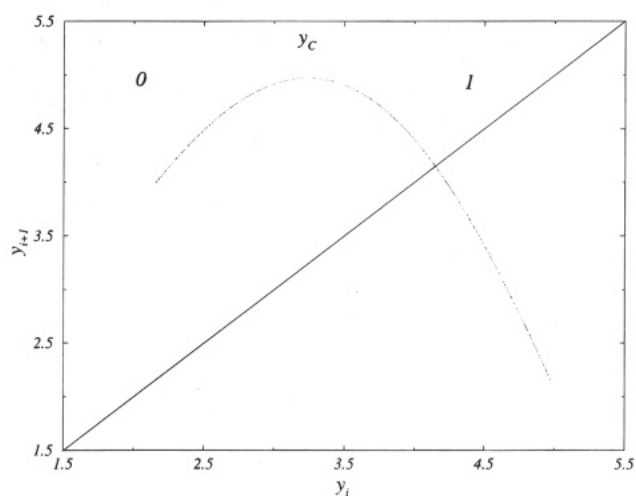


Figure 4. First-return map of the Rössler system: $(a, b, c) = (0.398, 2, 4)$.

decreasing branch associated with stripe 1. The critical point y_c which separates the branches precisely defines the partition. In our case, $y_c = -3.04$. Thus, at each intersection y_i with the Poincaré plane corresponds to a code $K(y_i)$:

$$K(y_i) = \begin{cases} 0 & \text{if } y_i > y_c \\ 1 & \text{if } y_i < y_c \end{cases} \quad (13)$$

Once periodic orbits are extracted by a Newton–Raphson iteration scheme, periodic points in the Poincaré section may be encoded. An orbit of period p has p periodic points and is represented by a string S of p codes:

$$S = K(y_1)K(y_2)\dots K(y_p)$$

where y_i s are the y coordinates of the periodic points.

3. *Unimodal Order.* Each period- p point is represented by a symbolic sequence of p symbols. Thus, the i th point of a period- p orbit is labeled by the string

$$S_i = K(y_i)K(y_{i+1})\dots K(y_p)K(y_1)\dots K(y_{i-1}) \quad (14)$$

All periodic points are then ordered by the unimodal order.^{33,34} **Definition.** The unimodal order \leq_1 on the symbol set 0,1 is defined as follows. Let

$$W_1 = \sigma_1 \sigma_2 \dots \sigma_k \sigma_{k+1} \dots$$

and

$$W_2 = \tau_1 \tau_2 \dots \tau_k \tau_{k+1} \dots$$

where σ_i s and τ_i s designate the codes. Suppose $\sigma_i = \tau_i$ for all $i < k$ and $\sigma_k \neq \tau_k$. Let $W^* = \sigma_1 \dots \sigma_{k-1} = \tau_1 \dots \tau_{k-1}$ be the common part between W_1 and W_2 . Assuming a string $\sigma_1 \sigma_2 \dots \sigma_{k-1}$ is even if the sum $\sum_{i=1}^{k-1} \sigma_i$ is even, and reciprocally (W^* is considered as even when no common part is found between W_1 and W_2), then

$$W_1 \leq_1 W_2 \text{ if } W^* \text{ is even and } \sigma_k < \tau_k$$

$$W_1 \leq_1 W_2 \text{ if } W^* \text{ is odd and } \tau_k < \sigma_k$$

$$W_2 \leq_1 W_1 \text{ if } W^* \text{ is odd and } \sigma_k < \tau_k$$

$$W_2 \leq_1 W_1 \text{ if } W^* \text{ is even and } \tau_k < \sigma_k$$

When $W_2 \leq_1 W_1$, we say W_1 implies W_2 .

A period- p orbit will be denoted by the symbolic sequence W_i (without any parentheses) which implies the $p - 1$ others. This sequence is noted (W_i) , included between parentheses, and here called *orbital sequence*. In a similar way, two orbital sequences may be ordered following the unimodal order. When orbital sequence (W_1) implies the orbital sequence (W_2) , we say that (W_1) forces (W_2) and we note $(W_2) \leq_2 (W_1)$ where \leq_2 is the forcing order.

In this way, all periodic orbits are ordered. The orbital sequence which forces all orbital sequences extracted from the attractor is called the *kneading sequence*. Within the Rössler attractor, the kneading sequence (among the orbits of period less than 12) is found to be (10111101010).³² All orbits forced by the kneading sequence are found up to period 11.

4. *Symbolic Plane.* With numerical systems, an orbit spectrum is always well-known within the limits imposed by round-off errors since orbits are extracted by integrating the vector field. Nevertheless, from experimental data, periodic orbits are extracted from a time series by using a close-return method in a reconstructed space. Due to the limited amount of data and the influence of external noise, the orbit spectrum is rarely well-known. As shown by Tuffillaro *et al.*³⁵, the population of periodic orbits depends in a crucial way on the length of the time series. Consequently, the determination of the kneading sequence is rather unprecise from short time series.

Fang³⁶ has shown that an empirical procedure (also used by Tuffillaro *et al.*³⁵) may exhibit the pruning front and, consequently, the kneading sequence. Let us recall that a chaotic trajectory forms a string

$$s = \dots \sigma_{-3} \sigma_{-2} \sigma_{-1} \sigma_0 \sigma_1 \sigma_2 \sigma_3 \dots$$

where σ_0 is the present, σ_{-i} the past, and σ_i the future ($i > 0$).

Symbolic coordinates which span a symbolic plane are defined on the future and the past as follows:

$$x_\sigma(s) = \sum_{i=1}^D \frac{b_i}{2^i}, \text{ where } b_i = \sum_{j=1}^i \sigma_j \pmod{2}$$

$$y_\sigma(s) = \sum_{i=1}^D \frac{c_i}{2^i}, \text{ where } c_i = \sum_{j=0}^{i-1} \sigma_{-j} \pmod{2} \quad (15)$$

where

$$s = \sigma_{-D} \dots \sigma_{-3} \sigma_{-2} \sigma_{-1} \sigma_0 \sigma_1 \sigma_2 \sigma_3 \dots \sigma_D$$

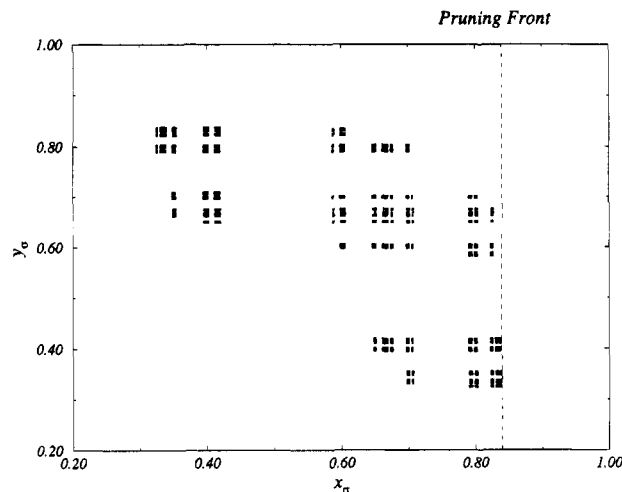


Figure 5. Symbolic plane of the Rössler attractor: orbit spectrum is governed by the unimodal order as shown by the pruning front well-estimated by a line.

If s is an infinite symbol string generated by a chaotic orbit, then D is infinity in the above definition. However, since we are dealing with finite data sets, Tuffillaro *et al.*³⁵ approximate the symbolic plane coordinates of a point by taking $D = 16$. In this way, we can use a finite symbol string from a chaotic trajectory to generate a sequence of points on the symbolic plane displayed in Figure 5. In the case of an orbit spectrum governed by the unimodal order, the pruning front is then suitably estimated by a line.³⁶

The symbolic coordinate X_σ of the pruning front allows us to define the kneading sequence. Indeed, by computing the symbolic points of periodic orbits, the kneading sequence is associated with the orbit whose maximum x_σ is closest to the pruning front. For reference, maximum symbolic coordinate x_σ of orbits with a period less than 9 are reported in Table 1. In the Rössler case, the pruning front is located at $x_\sigma = 0.8376$. From the orbit spectrum of the Rössler attractor, the kneading sequence is (10111101010) whose symbolic coordinate is found to be 0.8375. Good agreement is therefore obtained between the orbit spectrum and the symbolic plane.

From experimental data, the symbolic plane will be systematically used to check the orbit spectrum.

5. *Template Validation.* A template of the Rössler attractor has been proposed in section II.B.1. An orbit spectrum is extracted. Now, the template must be checked by comparing linking numbers predicted by the template and the ones counted on the attractor.

The linking number $L(N_1, N_2)$ of an orbit pair is given by the half-sum of the oriented crossings (following the convention, given in Figure 6, due to Melvin and Tuffillaro³¹) on a regular plane projection of orbits N_1 and N_2 . For example, linking number $L(1011, 1)$ is equal to -2 (Figure 7).

A comparison with the template-predicted linking number $L(1011, 1)$ is achieved by using an algebraic relation between symbolic dynamics and linking matrices according to³⁷

$$L(N_1, N_2) = \frac{1}{2} \left[\sum_{i=1}^{p_1} \sum_{j=1}^{p_2} M(\sigma_i, \sigma_j) + N_{\text{lay}}(N_1, N_2) \right] \quad (16)$$

where N_1 and N_2 are two orbits of period p_1 and p_2 , respectively. $M(\sigma_i, \sigma_j)$ are the linking matrix elements, and $N_{\text{lay}}(N_1, N_2)$ is the layering number determined by using a layering graph (sketched in Figure 8 for the couple (1011, 1), see ref 37 for details).

TABLE 1: Greatest x_σ -Coordinate of Orbits Whose Period is Less Than 9, Ordered Following the Forcing Order

W	$x_\sigma(W)$	W	$x_\sigma(W)$
1	0.66665	10011010	0.92547
10	0.79998	10011011	0.92605
1011	0.82351	1001101	0.92912
10111010	0.82489	1001100	0.93022
101110	0.82539	1001	0.93331
101111	0.83076	1000	0.94116
10111110	0.83135	10001001	0.94161
10111111	0.83267	1000100	0.94486
1011111	0.83464	1000101	0.94572
1011110	0.83720	10001011	0.94900
10111	0.83869	10001010	0.94940
10110	0.84848	100010	0.95237
1011010	0.85038	100011	0.95384
1011011	0.85270	10001110	0.95684
10110111	0.85488	10001111	0.95718
10110110	0.85601	1000111	0.96061
101	0.85713	1000110	0.96122
100	0.88888	10001101	0.96469
100101	0.89230	10001100	0.96496
10010110	0.89410	10001	0.96772
10010111	0.89492	10000	0.96969
1001011	0.89762	10000100	0.97253
1001010	0.89921	10000101	0.97274
10010101	0.90194	1000010	0.97636
10010100	0.90270	1000011	0.97673
10010	0.90321	10000111	0.98037
10011	0.90908	10000110	0.98052
10011100	0.90979	100001	0.98411
10011101	0.91049	100000	0.98460
10011110	0.91337	10000010	0.98822
10011111	0.91471	10000011	0.98831
100111111	0.91763	1000001	0.99211
100111110	0.91827	1000000	0.99223
100111	0.92062	10000001	0.99606
100110	0.92306	10000000	0.99609

In the present case, we obtain:

$$L(1011,1) = \frac{1}{2}[3M(1,1) + M(1,0) + N_{\text{lay}}(1011,1)]$$

$$= \frac{1}{2}[-3 - 1 + 0] = -2 \quad (17)$$

i.e., the template linking number $L(1011,1)$ is the same as that on the attractor; the template is therefore compatible with the attractor. In utmost rigor, a few linking numbers are needed to completely check the template.

As the template which carries the periodic orbits is identified, the organization of the orbits within the attractor is known. For a complete discussion about equivalence between periodic orbits embedded within a strange attractor and orbits of the template, see ref 38.

If time series generated by a model and an experiment, embedded in the same way in a three-dimensional manifold, induce the same template, the model is compatible with the data. If different templates are induced, the model cannot provide a valid description of the processes generating the experimental time series.

III. Copper Electrodeposition

A. Characterization of the Electrochemical Reaction.

Copper electrodeposition in H_3PO_4 has been studied by Albahadily and Schell⁹ and has been found to undergo Hopf bifurcation to oscillatory behavior followed by period-doubling bifurcations to simple chaos. As studied by Coulet and Tresser³⁹ and Feigenbaum,⁴⁰ this simple chaos is characterized by a unimodal first-return map on a Poincaré section, i.e., with two monotonic branches, one increasing and one decreasing,

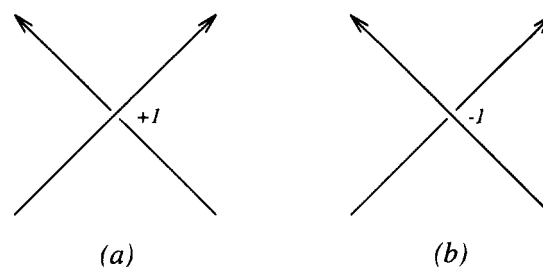


Figure 6. Crossing convention: (a) positive crossing and (b) negative crossing.

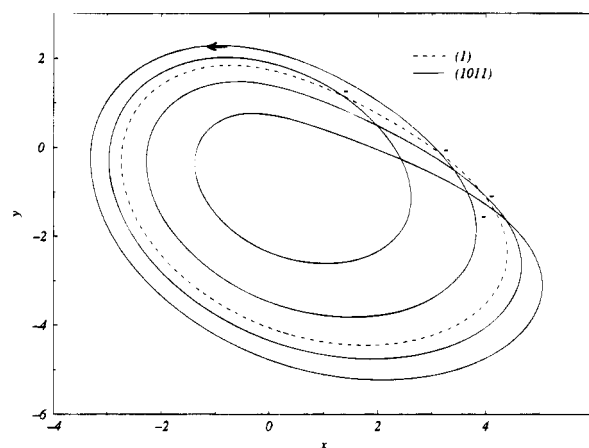


Figure 7. Plane projection of the orbit couple (1011,1). The linking number $L(1011,1) = \frac{1}{2}[-4] = -2$. Crossings are signed by inspection on the third coordinate.

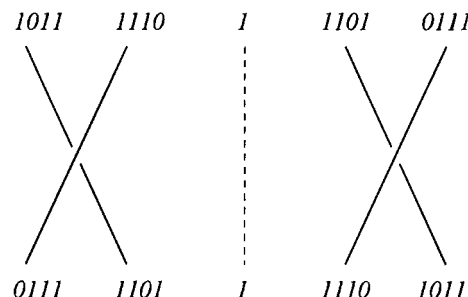


Figure 8. Layering graph between (1) and (1011). Lower base is given by the unimodal order of periodic points. Upper base is obtained by permutating periodic points of stripe 1 (whose symbolic sequences begin by a "1") since stripe 1 has an odd number of π twists. Periodic points of stripe 1 are thereafter permutated with periodic points of stripe 0 since the intersection number $M(1,0)$ between stripe 1 and stripe 0 is odd. The layering number $N_{\text{lay}}(1011,1)$ is equal to the sum of the intersections between (1011) and (1) (self-intersections are not taken into account). Here $N_{\text{lay}}(1011,1)$ is null.

separated by a maximum differentiable point. This chaos will be completely characterized in this section.

1. Experiment. The time series was obtained from dissolution current measurement during the potentiostatic electrodis-solution of a rotating Cu electrode in phosphoric acid. The experimental setup consisted of a rotating disc electrode which had a copper rod, 8.26 mm in diameter, embedded in a 2 cm diameter Teflon cylinder. The rotating speed was maintained at 4400 rpm. In order to minimize noise, we used a mercury contact instead of a standard silver-carbon brush contact.⁴¹ A cylindrical platinum net band (much larger than the disc) was put around the disk as a counter electrode to get uniform potential and current distributions.

The cell was a 500 mL flask with a side neck in which the capillary probe was fixed. The reference electrode was SCE, which was separated from the solution by the capillary. The

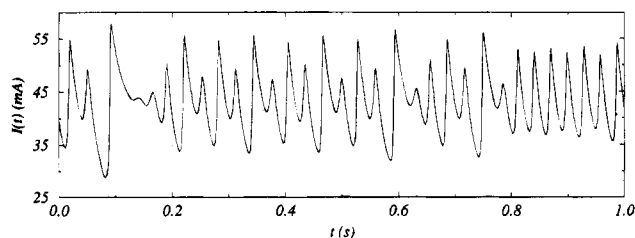


Figure 9. Current-time series $I(t)$.

distance between the disc surface and the tip of the capillary was about 6 mm. The cell contained 250 mL of 85% phosphoric acid, and a water bath was used to maintain its temperature at 20 °C.

A Potentiostat (Princeton Applied Research Model 273) was used to regulate the potential of the working disc electrode with respect to the SCE and to monitor the current. The data were recorded at a frequency f_e of 1500 Hz using a 486 PC and a data acquisition board (Model DAS-16, Keithley Metrabyte's). The current-time series $I(t)$ is displayed in Figure 9.

After the initial transient signal disappeared, the behavior settles down to a chaotic attractor in the state space.

By using a reconstruction method as proposed by the pioneering paper by Packard *et al.*,¹¹ such an attractor may be reconstructed from the current-time series in a space spanned by derivative coordinates. In order to do that, we have to estimate the dimension m of the reconstructed state space. This may be achieved by using the well-known algorithm proposed by Grassberger and Procaccia⁴² which estimates the correlation dimension D_2 : m may be taken to be equal to the first integer greater than D_2 . From the current-time series $I(t)$, we found $D_2 = 2.3 \pm 0.2$. Therefore, a tridimensional space should be sufficient to obtain a good representation of the attractor generated by the copper electrodisolution.

We assume (and shall prove) that the current $I(t)$ is a good observable, i.e., the reconstructed attractor in the tridimensional space spanned by the derivative coordinates is at least topologically equivalent to the original unknown attractor. The copper electrodisolution may then be modeled by a set of three equations and the corresponding attractor reconstructed in a tridimensional space spanned by the derivative coordinates is generated by

$$\begin{aligned} X &= I(t) \\ Y &= \dot{I}(t) \\ Z &= \ddot{I}(t) \end{aligned} \quad (18)$$

A projection in the XY plane of the attractor is displayed in Figure 10. Successive time derivatives of the current-time series $I(t)$ are estimated by using the linear filter built on a Legendre polynomial basis (as described in section II.A). The window size τ_w used to estimate the derivatives is taken to be equal to 21τ (where $\tau = f_e^{-1}$).

2. *Orbit Spectrum.* The attractor presents a "hole" in its middle which warrants the existence of a Poincaré plane and the possibility of easily constructing a first-return map without any ambiguity. The Poincaré section P is defined as follows:

$$P \equiv \{(X, Y) \in \mathbb{R}^2 | X = 43.7, Y > 0\} \quad (19)$$

The first-return map from the Poincaré section P to itself is displayed in Figure 11. The map is almost unidimensional, which is a signature of the strongly dissipative character of the dynamics. A unimodal map with a unique maximum is obtained.

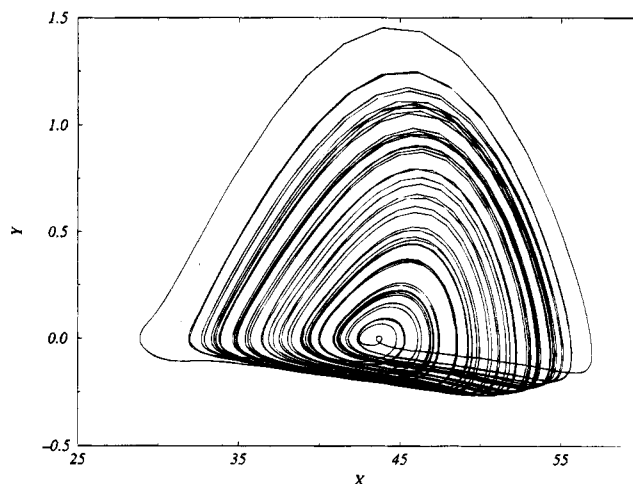


Figure 10. Projection in the XY plane of the attractor generated by the copper electrodisolution.

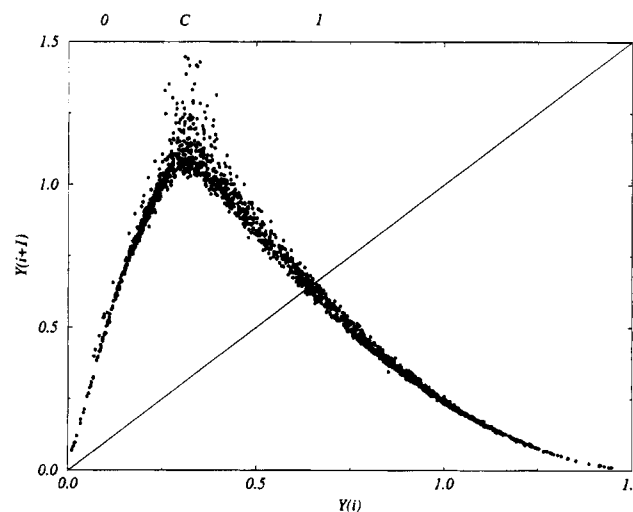


Figure 11. First-return map on the Poincaré section P .

The critical point C allows the definition of a symbolic dynamic as follows:

$$\begin{aligned} 0 &\text{ if } Y < 0.32 \\ 1 &\text{ if } Y > 0.32 \end{aligned} \quad (20)$$

The population of periodic orbits is then extracted from the current-time series $\{I_n\}_{n=1}^{300000}$, where n is a discretized time in terms of τ . The Poincaré set is then constituted by 1949 points. The population of periodic orbits which is extracted by a close return method is reported in Table 2.

Orbits are found with a close-return less than 1% of the attractor size. Up to period 7, all periodic orbits forced by the sequence (100110) with respect to the forcing order \leq_2 are found. By plotting the symbolic plane, the greatest symbolic coordinate X_σ is found to be equal to 0.9250, which also implies the kneading sequence (100110) (see Table 1). A good agreement is therefore obtained between the symbolic plane and the orbit spectrum. The attractor is governed by the unimodal order; this is consistent with the period-doubling cascade as a route to chaos, observed by Albahadily and Schell.⁹

Nevertheless, one may remark that the pruning front is not well-estimated by a line as requested by a system which is governed by the unimodal order. This is not very surprising in so far as the experimental first-return map is not perfectly unidimensional. However, a well-visited zone may be exhibited

TABLE 2: Orbits Spectrum of the Copper Attractor. ● Designates Orbits Found within the Experimental Attractor A_C , ○ Orbits Found Within the Reconstructed Attractor A_R . Kneading Sequences are Designed by a Double Symbol. Orbits are Found with an Error Less Than 1.00% of the Attractor Size

period	sequence	A_C	A_R
1	1	●	○
	0	●	
2	10	●	○
3	101	●	
	100	●	
4	1011	●	○
	10110	●	○
5	10010	●	○
	10011	●	○
	101110	●	○
	101111	●	○
	100101	●	○
6	100111	●	
	100110	●	
	1011110	●	○
	1011111	●	○
	1001010	●	
	1001011	●	
	1001101	●	
	1001110	●	
	1001111	●	
	1011010	●	
7	1011011	●	○
	1011110	●	○
	1011010	●	
	1011011	●	
	1001011	●	
	1001010	●	
	1001110	●	
	1001111	●	

up to $x_0 = 0.8420$. A small number of points are found in the range $[x_0, X_\sigma]$, representing ten of the total set.

Considering the first-return map in Figure 11, a natural invariant density $\varrho(Y)$ which indicates the frequency of visits to any given interval of the Poincaré section may be estimated.^{43,44} $\varrho(Y)$ may be computed as a numerical histogram approximation. In the ideal theoretical case, it is shown that singularities of $\varrho(Y)$ are produced at iterates of the critical point.⁴⁴ Consequently, $\varrho(Y)$ exhibits sharp peaks associated with the kneading sequence since the periodic orbit encoded by the kneading sequence is generated by the critical point.

The invariant density for the Rössler attractor is exhibited in Figure 13a, indeed displaying the kneading sequence singularities. The invariant density for the experimental copper attractor is conversely displayed in Figure 13b. Although the Rössler and the copper attractor possess the same orbit spectrum, one may remark that the invariant density of the copper attractor vanishes progressively on the tails of the distribution in contrast with the Rössler attractor case where high-amplitude discrete peaks are observed at the distribution frontiers. We may assume that such differences result from the fact that the copper map is not perfectly 1D but is built from a 1D ideal behavior on which a noisy component is superimposed. This noisy component in particular produces the tails in Figure 13b, associated with zones on the periphery of the attractor which are rarely visited. Such zones are also visible in the symbolic plane in the range $[x_0, X_\sigma]$ of Figure 12. We shall return to this point later to give better support for this assumption.

3. Template. Topological characterization of the copper attractor may now be achieved. According to the first-return map to the Poincaré section P , the template is constituted by two stripes: one stripe whose local torsion is even and which is associated with the increasing branch 0 and one stripe whose local torsion is odd and which is associated with the decreasing branch. From the inspection of the attractor in a 3D phase space, it is found that the two stripes are organized as displayed in Figure 14. Stripe 0 is found without any local torsion, and stripe 1 is found with a $+\pi$ twist, i.e., like a so-called Möbius band.

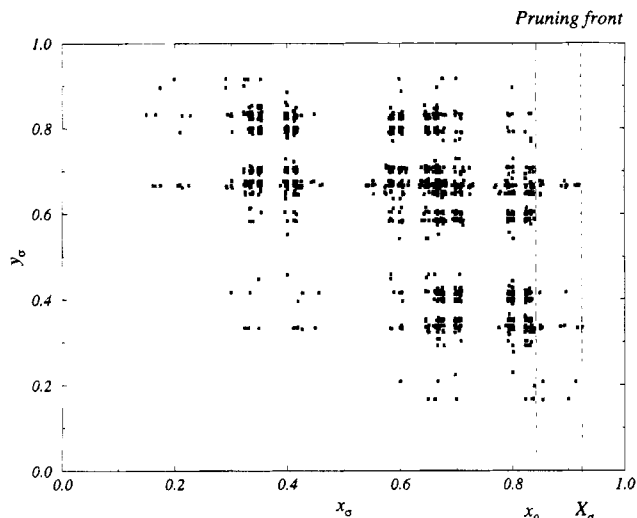


Figure 12. Symbolic plane of the copper attractor. Pruning front has a coordinate $X_\sigma(E) = 0.9250$ which confirms that the last periodic orbit to appear is the orbit encoded by (100110). A low-visited zone appears between the dashed lines.

We then propose the template displayed in Figure 15 as representative of the copper attractor. Its linking matrix reads

$$M_{cop} \equiv \begin{pmatrix} 0 & 0 \\ 0 & +1 \end{pmatrix} \quad (21)$$

The template is now checked by counting the oriented crossings of a few orbit couples on a plane projection. We use (10,1) and (1011,10) couples. Linking numbers $L(10,1)$ and $L(1011,10)$ are found to be equal to +1 and +3, respectively (Figures 16a and 16b).

By using the algebraic relation 16, we obtain

$$\begin{aligned} L(10,1) &= \frac{1}{2}[M(1,1) + M(1,0) + N_{lay}(10,1)] \\ &= \frac{1}{2}[1 + 0 + 1] = +1 \end{aligned}$$

$$\begin{aligned} L(1011,10) &= \frac{1}{2}[3M(1,1) + 4M(1,0) + M(0,0) \\ &\quad + N_{lay}(1011,10)] \\ &= \frac{1}{2}[3 + 0 + 0 + 3] = +3 \end{aligned} \quad (22)$$

where $N_{lay}(1,10)$ and $N_{lay}(1011,10)$ are the layering numbers obtained from the layering graphs displayed in Figures 16c and 16d. Linking numbers counted on plane projections and induced by the template are equal, i.e., the template is therefore checked.

B. Reconstructed Model. Since the dynamics of the original attractor have now been characterized, the next goal is the reconstruction of a set of equations modeling the experimental behavior. In order to obtain a reconstructed global vector field, we apply the reconstruction method of section II.A to the data of the copper electrodisolution. As stated in section II.A, successive derivatives of the time series $I(t)$ are required. They are estimated by using the discrete Legendre filter with a window size $\tau_w = 21\tau$. In order to obtain successful integrations of the reconstructed system, we found that the data set should be constituted by a trajectory which visits the periphery of the attractor. Typically, from any such a set, two kinds of dynamics

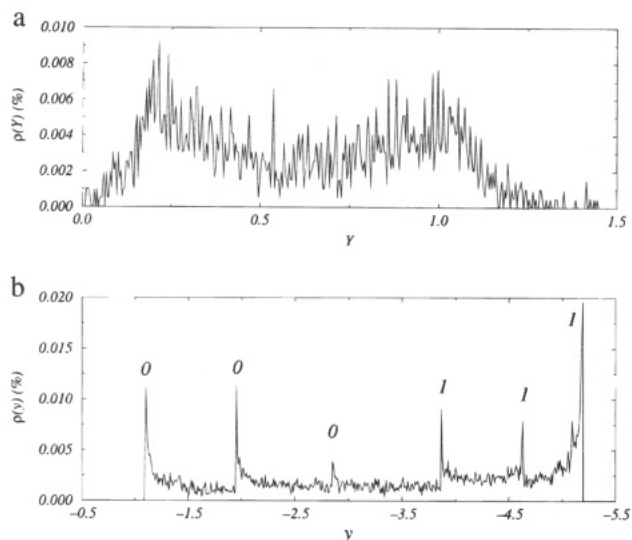


Figure 13. Comparison between the density computed from the copper attractor and the one computed from the Rössler attractor with an identical orbit spectrum, $(a,b,c) = (0.422,2,4)$. As suggested by theoretical results, Rössler density presents two peaks on the limits of the invariant interval: these peaks provide a signature of the kneading sequence. Copper density suggests that limits of the invariant interval are not well defined. (a) Copper attractor. (b) Rössler attractor.

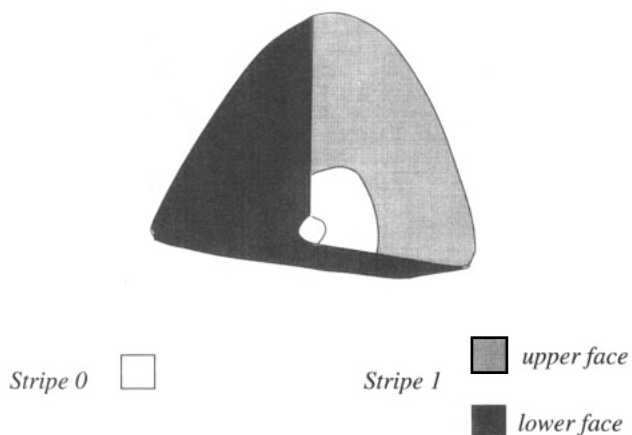


Figure 14. Two stripes are exhibited on the attractor: stripe 0 without local torsion and stripe 1 with a $+\pi$ twist. No intersections are found between the two stripes.

may be reconstructed: (i) a chaotic attractor with the driving vector $(\tau, 295, 14, 52, 21\tau)$ (Figure 17); (ii) a limit cycle of period 6 with the driving vector $(\tau, 470, 61, 51, 21\tau)$ (Figure 18), i.e., with a larger amount of data than for the chaotic attractor. This limit cycle is encoded by the sequence (100110) and, consequently, corresponds to the kneading sequence of the copper attractor. Here, the driving vectors are found by using an error function E_r minimization as previously explained.

It is not yet well understood how the quality of the reconstructed model depends on the reconstruction parameters. Nevertheless, it is shown⁴⁵ that the amount of vectors used in the approximation may act as a control parameter on the dynamics.

In our case, the limit cycle is reconstructed by using 470 net points sampled on about 8 pseudoperiods of the data series. During 6 of these pseudoperiods, the chaotic trajectory remains topologically very close to the period-6 limit cycle encoded by the sequence (100110). As (100110) is the kneading sequence of the copper attractor, in spite of the visual appearance, this periodic behavior is actually very close to the experimental one (in so far as a slight variation of the control parameter is

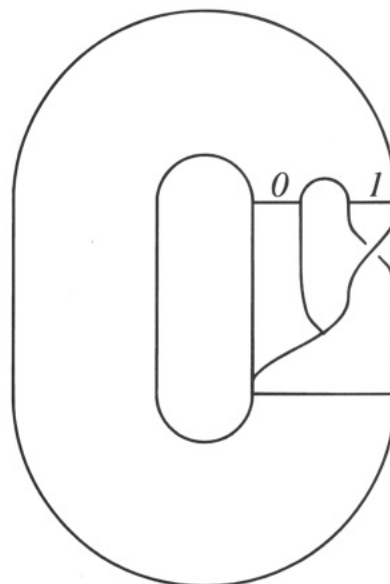


Figure 15. Template of the copper attractor.

sufficient to pass from the chaotic behavior to the periodic behavior, and vice versa).

The reconstructed chaotic attractor is obtained with 295 net points (a small amount of data indeed) sampled on about 21 pseudoperiods of the data series. Those points are on a chaotic trajectory which sufficiently visits the attractor so that the driving vector $(\tau, 295, 14, 52, 21\tau)$ permits reconstruction of a chaotic attractor which will be characterized and compared to the original one in the next section.

Values of K_s generating the chaotic strange attractor are reported in Table 3.

The reconstructed systems are integrated with an adaptive step integrator. The reconstructed chaotic attractor obtained by integrating the reconstructed vector field is displayed in Figure 17. In the remainder of this paper, we call the *copper attractor* the chaotic attractor A_c reconstructed by using the successive derivatives from experimental data and the *reconstructed attractor* the attractor A_R generated by integrating the reconstructed vector field.

In order to check the model generated by the reconstructed vector field, a complete analysis is now performed on the reconstructed attractor A_R .

1. Orbit Spectrum. The first-return map of the reconstructed attractor is computed on the same Poincaré plane as for the copper attractor and is displayed in Figure 19.

The map is a bit less developed than the original one. As should have been expected, the reconstructed map is one-dimensional, i.e., the thickness of the experimental Poincaré section is completely removed. The population of periodic orbits is extracted and reported in the fourth column of Table 2. All extracted periodic orbits are forced by the kneading sequence (10110) of A_R . All sequences forced by this sequence are found within the reconstructed attractor. The symbolic plane (Figure 20) then provides a pruning front, correctly estimated by a line, at $X_\sigma = 0.8450$, which is in good agreement with the symbolic coordinate of the kneading sequence (0.8485).

Also, the natural invariant density (Figure 21) of the map presents sharp peaks generated by the periodic points of the kneading sequence, as theoretically expected.

We therefore observe that the orbit spectrum of the reconstructed attractor is pruned with respect to the copper attractor. Nevertheless, one must remark that the pruning front of the

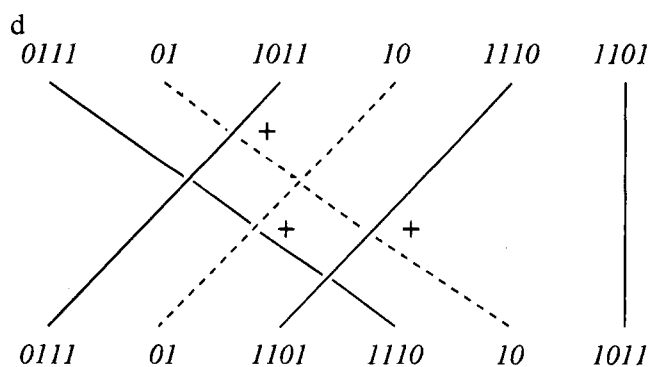
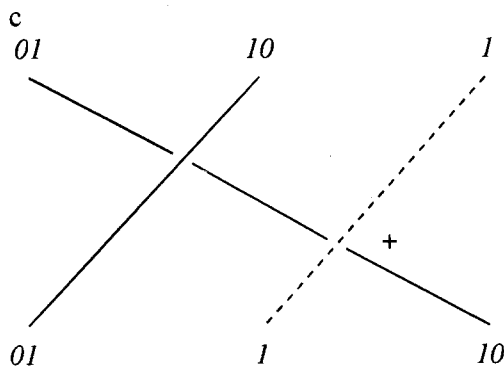
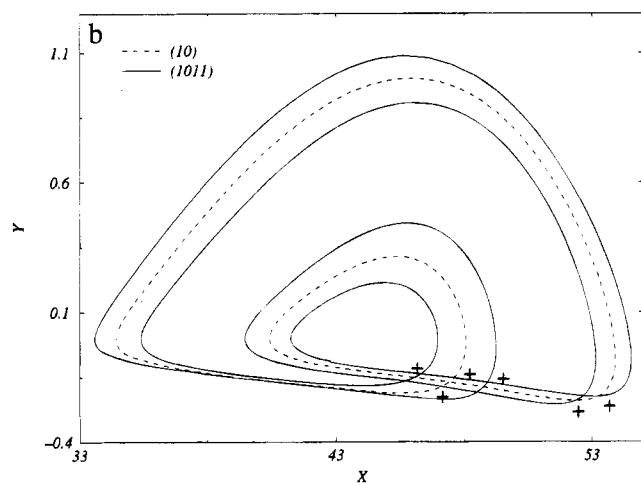
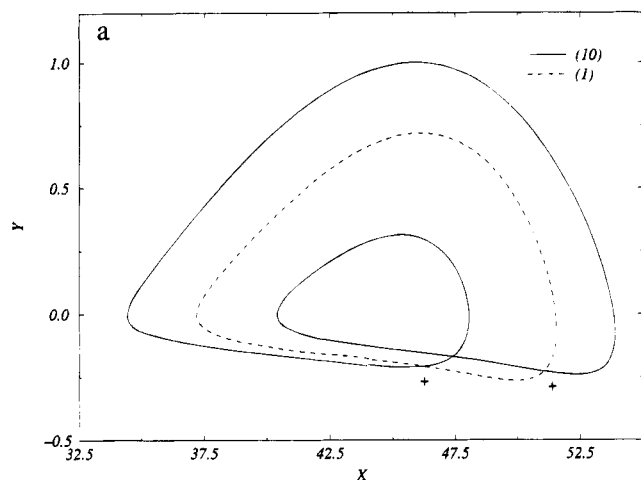


Figure 16. Plane projections and layering graphs of two orbit couples. The lower bases of the layering graphs are built on the unimodal order while the upper base is obtained by reversing the order of periodic points of the stripe 1 since $M(1,1)$ is odd. No permutating between periodic points of the stripe is required since $M(1,0)$ is even. (a) $L(10,1) = +1$. (c) $L(1011,10) = +3$. (b) $N_{\text{lay}}(10,1) = +1$. (d) $N_{\text{lay}}(1011,10) = +3$.

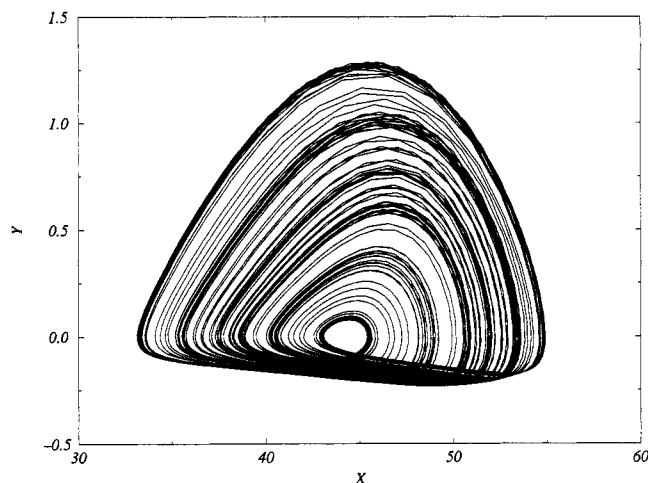


Figure 17. Reconstructed attractor A_R of the copper electrodisolution by integrating the reconstructed vector field driven by the vector $(\tau, 295, 14, 52, 21\tau)$; projection in the XY plane.

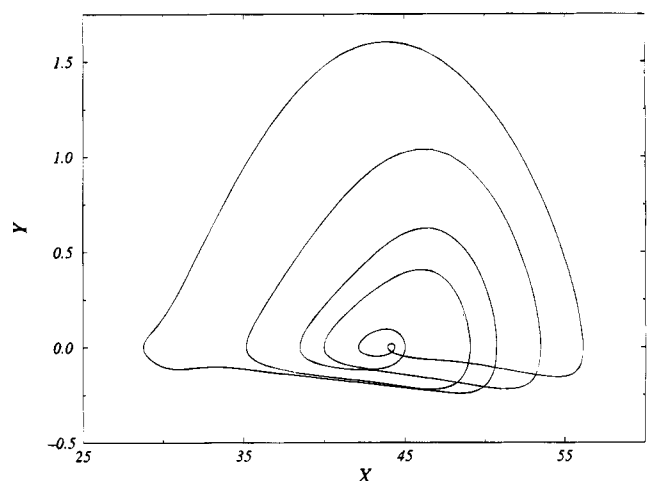


Figure 18. Reconstructed limit cycle of the copper electrodisolution by integrating the reconstructed vector field driven by the vector $(\tau, 470, 61, 51, 21\tau)$; projection in the XY plane. The limit cycle is encoded by (100110) .

reconstructed attractor (0.8450) is very close to the limit of the well-visited zone (0.8420) in the symbolic plane of the copper attractor. Indeed, the orbit spectrum found within the reconstructed attractor is identical to the one corresponding to the well-visited zone of the copper attractor.

We now recall that the reconstructed system is extracted from experimental data and that there are several factors which complicate the reconstruction problem from experimental data:¹⁶ (i) Observational noise, the measuring instrument may be noisy; we actually observe a time series $I(t)$ given by

$$I(t) = \tilde{I}(t) + \xi(t) \quad (23)$$

where $\tilde{I}(t)$ is the true value and $\xi(t)$ is noise. (ii) Dynamic noise, external influences may perturb the dynamics; the evolution of the system is not only deterministic but also possesses a stochastic component. This kind of noise is numerically well simulated by a multiplicative noise as follows

$$\dot{x} = f(x + \xi(t)) \quad x, \xi \in \mathbb{R}^n \quad (24)$$

where x is the state vector, f the vector field, and $\xi(t)$ is noise. (iii) Estimation error, with a finite amount of data, the reconstructed vector field is an estimation which never can be

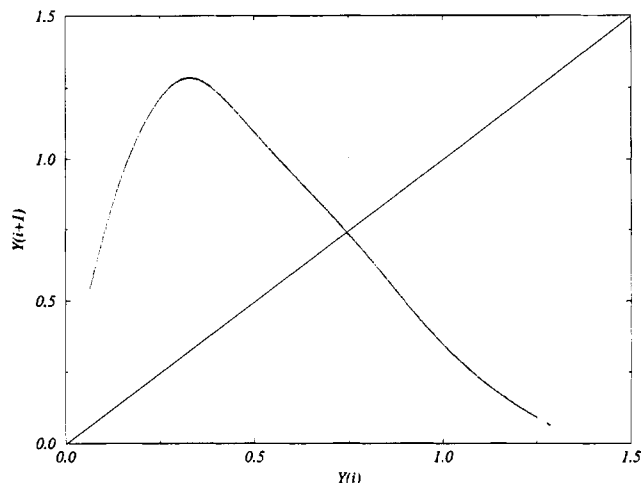


Figure 19. First-return map on the Poincaré section P of the reconstructed attractor A_R .

TABLE 3: Values of K_i Given by a Reconstruction Driven by the Vector $(\tau, 295, 14, 52, 21\tau)$; Integration of the Reconstructed System Generates a Chaotic Attractor

l	K_l	l	K_l
1	0.1219705394981005	27	-0.145539951745097
2	-1.078249529843902 $\times 10^{-2}$	28	0.1049018763188871
3	0.9125082050943352	29	12.14985173080021
4	-31.5804652088144	30	-38.5366235437547
5	2.882119184023051 $\times 10^{-4}$	31	0.3809613670493999
6	-0.107945627123624	32	2.19570526400687
7	3.14261019012943	33	21.55254081698994
8	-2.58142102535676	34	165.1484278847694
9	30.7789877436226	35	-1437.72802782965
10	180.3217927930279	36	7.928626337606531 $\times 10^{-10}$
11	-5.550910841337609 $\times 10^{-7}$	37	5.752046655223851 $\times 10^{-7}$
12	4.625376454207544 $\times 10^{-3}$	38	-1.081602890433014 $\times 10^{-5}$
13	-0.114822275266309	39	4.628712833151052 $\times 10^{-5}$
14	0.2121650714651616	40	-3.976058731703460 $\times 10^{-4}$
15	-2.24124505814176	41	-2.626758361863347 $\times 10^{-3}$
16	-13.6799701248913	42	1.437994615429103 $\times 10^{-3}$
17	3.60656873135868	43	1.753989520753347 $\times 10^{-4}$
18	-6.67239615224999	44	-0.126567212485869
19	-287.70105676069	45	0.3435285584041194
20	1083.030601671941	46	-5.116362209078044 $\times 10^{-3}$
21	-7.711227398599053 $\times 10^{-8}$	47	-3.788259242947936 $\times 10^{-2}$
22	-8.541800526483852 $\times 10^{-5}$	48	-0.572245746550728
23	1.833011097559745 $\times 10^{-3}$	49	-4.44596569136184
24	-5.532917786559483 $\times 10^{-3}$	50	23.99099286766239
25	5.276461759803514 $\times 10^{-2}$	51	-8.936897340164367 $\times 10^{-2}$
26	0.3345112248727262	52	-0.464973703176679

perfect; with the true vector field f being unknown, the estimation error is furthermore somewhat difficult to evaluate.

In the case of the copper experiment, the resolution of the data acquisition board is of 4096, i.e., the measuring instrument error is 1 part in 4096 and can be safely neglected.

In contrast, it is well known that intrinsic (dynamic) noise acts as a disordering field.⁴³ As a matter of fact, integrating the Rössler system (with the control parameters $(a,b,c) = (0.340,2,4)$ which correspond to the period-2 limit cycle of the period-doubling cascade) with a multiplicative noise (signal/noise ratio of 44 dB) provides a rather well-developed chaos.⁴⁵ Thus, small dynamic perturbations may have a great influence on the dynamics of a system.

As shown by Crutchfield *et al.*,⁴³ dynamic noise perturbs the natural invariant density by removing the sharp peaks produced at the iterates of the critical point, supporting the assumption discussed at the end of section III.A.2. This behavior is illustrated by taking the example of the Rössler system.

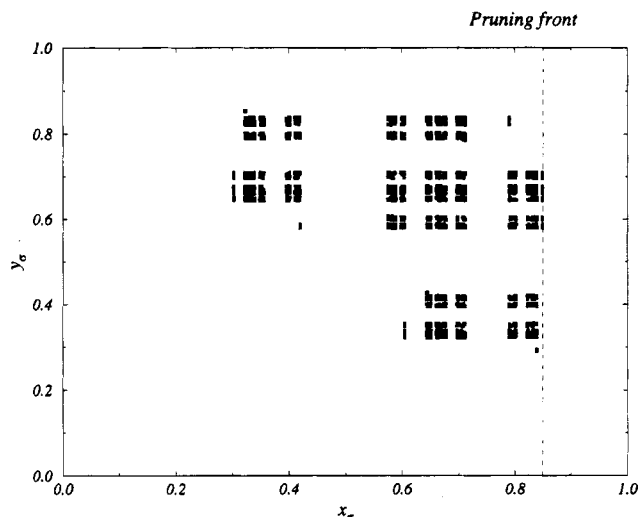


Figure 20. Symbolic plane of the reconstructed attractor. Pruning front is found at $X_\sigma = 0.8450$ and is suitably estimated by a line; dynamics is governed by the unimodal order.

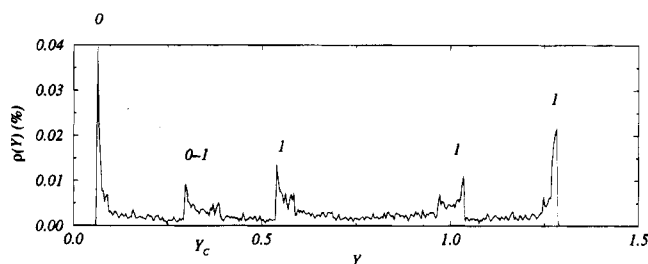


Figure 21. Natural invariant density. Each peak is labeled following the symbolic dynamics; sequences $(1011)_0^1$ of the couple created by a saddle-node bifurcation is exhibited.

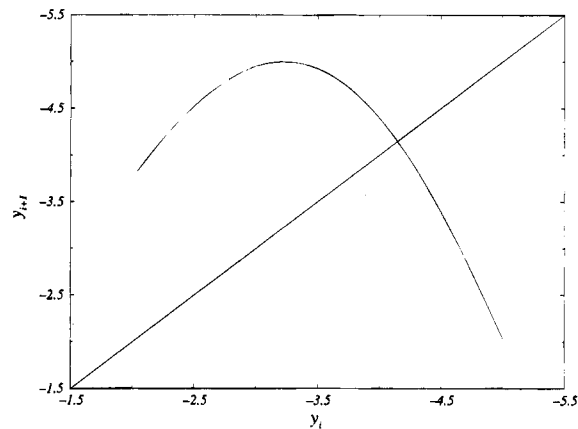


Figure 22. First-return map of the Rössler attractor whose orbit spectrum is forced by the sequence (10110) .

We start from a Rössler attractor whose orbit spectrum is the same as the reconstructed attractor one, i.e., with (10110) as the kneading sequence. Such an attractor is obtained for $(a,b,c) = (0.401,2,4)$. The first-return map is displayed in Figure 22.

We afterward integrate the Rössler system $((a,b,c) = (0.401,2,4))$ with a multiplicative noise as defined by relation 24 with a signal/noise ratio of 64 dB. The first-return map (Figure 23) now exhibits a significant thickness and presents more developed branches than the clean one (Figure 22).

The symbolic plane is computed (Figure 24). The maximum x_σ coordinate is found to be equal to 0.9166 (against 0.8485 without any noise) and the pruning front is not well defined by

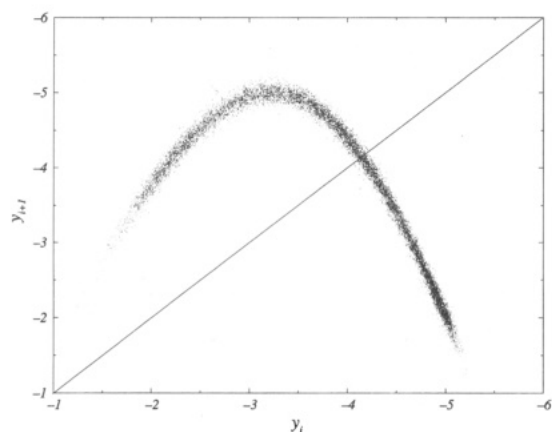


Figure 23. First-return map of the Rössler system ($a = 0.401$) integrated with a multiplicative noise of 64 dB.

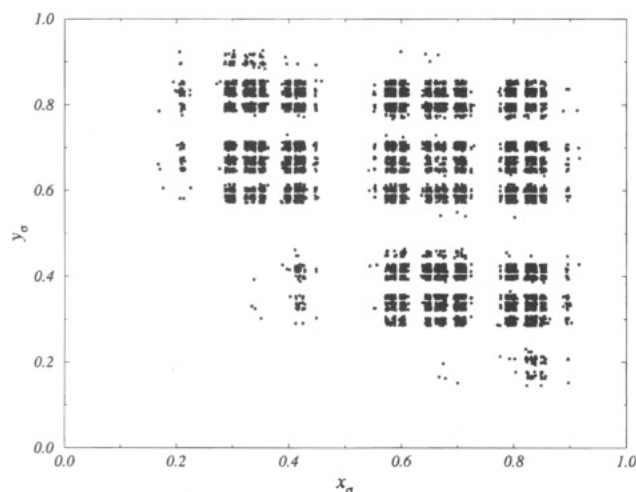


Figure 24. Symbolic plane of the noisy Rössler attractor ($a = 0.401$, $Sb \approx 64$ dB): a low-visited zone is exhibited as on the symbolic plane of the copper dynamics.

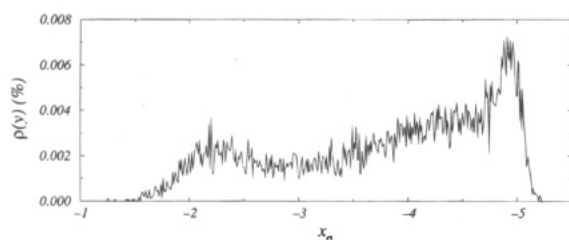


Figure 25. Natural invariant density $\bar{\rho}(y)$ of the noisy Rössler system. Sharp peaks are removed by the action of the noise and the tails of the distribution are not well defined.

a line. Moreover, a rarely-visited zone appears in the range $0.8598 < x_\sigma < 0.9166$. The rarely-visited zone on the copper attractor is in the range $0.8420 < x_\sigma < 0.9250$. The symbolic plane of the noisy Rössler attractor may therefore favorably compare with the copper attractor symbolic plane. Chaos is then developed on the noisy Rössler system in a way very similar to that of the copper attractor chaos. This is further supported by examining the natural invariant density of the noisy Rössler attractor (Figure 25) which is indeed well reminiscent of the one displayed for the copper experimental data in Figure 13b.

Also, the reconstructed vector field has been integrated with a multiplicative noise (relation 24) with the signal/noise ratio equal to 44 dB. The trajectory now visits the center of the copper attractor (Figure 26). In particular, the small loop in the hole of the attractor of Figure 26 which is present too in the experimental copper attractor (Figure

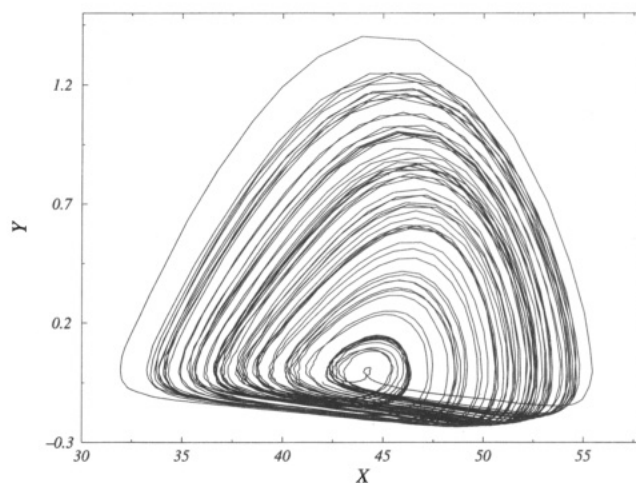


Figure 26. Attractor generated by the integration of the reconstructed global vector field with a multiplicative noise (signal/noise ratio equal to 44 dB).

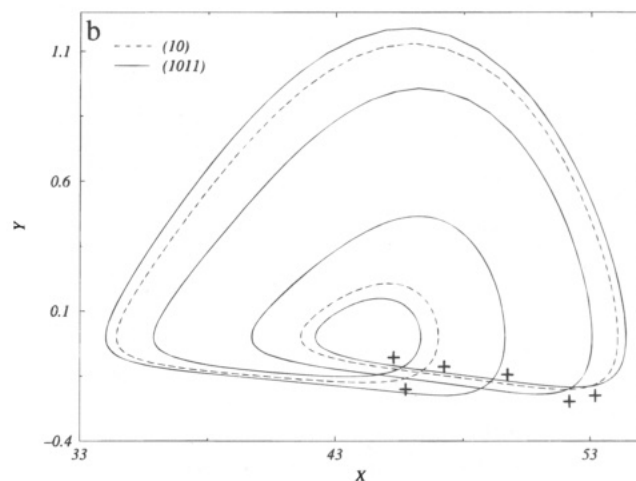
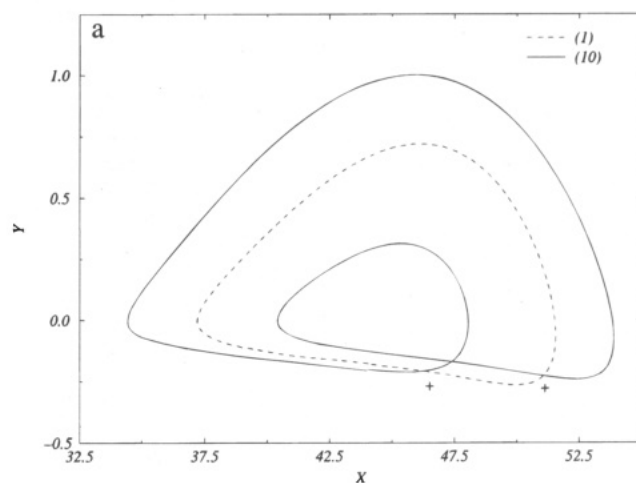


Figure 27. XY plane projection of the couples of periodic orbits. (a) $L(10,1) = {}^{1/2}L(+2) = +1$. (b) $L(1011,10) = {}^{1/2}L(+6) = +3$.

10) and on the kneading orbit of Figure 18 is never observed in the chaotic reconstructed attractor without any noise (Figure 17).

We therefore conclude that the copper attractor favorably compares to a Rössler attractor whose orbit spectrum is forced by the kneading sequence (10110) with a stochastic component modeled by a multiplicative noise of the order of 64 dB.

2. Template Validation. The relative organization of the periodic orbits obtained from the reconstructed model must now

be checked against the copper template. This is achieved with the two previously used couples of orbits, namely (10,1) and (1011,10). Linking numbers $L(10,1)$ (Figure 27a) and $L(1011,10)$ (Figure 27b) are found to be equal to +1 and +3, respectively. They are therefore equal to the ones predicted by the template of the copper attractor (relation 22). The reconstructed model is therefore topologically compatible with the data.

IV. Conclusion

We have demonstrated how vector field reconstruction can be applied to chaotic data from an electrochemical reaction, the electrodisolution of copper in phosphoric acid. A set of ordinary differential equations (ODE) has been generated in this manner, and this set is a model of the underlying physical system. The ODE set can be used to extract information about the dynamics of the process. Other methods are available to approximate the long-term dynamics of continuous time systems. Many of these approaches employ discrete maps with local linearization^{13,46} or ANNs,^{47,48} ANN coupled with a simple integrator scheme has also been employed.⁴

Acknowledgment. This work was supported in part by the National Science Foundation and by ARPA/ONR.

References and Notes

- Hudson, J. L.; Tsotsis, T. T. Electrochemical Reaction Dynamics: A Review. *Chem. Eng. Sci.* **1994**, *49* (10), 1493–1572.
- McAvoy, T. J.; Wang, N. S.; Naidu, S.; Bhat, N. V.; Gunter, J.; Simmons, M. Interpreting Biosensor Data via Back Propagation; *Proc. Int. Joint Conf. Neural Networks*: Washington, DC, 1989; Vol. 1, pp 227–233.
- Hudson, J. L.; Kube, M.; Adomaitis, R. A.; Kevrekidis, I. G.; Lapedes, A. S.; Farber, R. M. Nonlinear Signal Processing and System Identification: Applications to Time Series from Electrochemical Reaction. *Chem. Eng. Sci.* **1990**, *45* (8), 2075–2081.
- Rico-Martínez, R.; Krischer, K.; Kevrekidis, I. G.; Kube, M. C.; Hudson, J. L. Discrete- vs Continuous-Time Nonlinear Signal Processing of Cu Electrodisolution Data. *Chem. Eng. Commun.* **1992**, *118*, 25–48.
- Otawara, K.; Fan, L. T. Synchronizing Chemical Chaos with an Artificial Neural Network. Submitted to *J. Phys. Chem.*
- Jacquet, P. *Bull. Soc. Chim. Fr.* **1936**, *3*, 307.
- Glarum, S. H.; Marshall, J. H. The Anodic Dissolution of Copper into Phosphoric Acid. *J. Electrochem. Soc.* **1985**, *132*, 2872.
- Tsitsopoulos, L. T.; Tsotsis, T. T.; Webster, I. A. An Ellipsometric Investigation of Reaction Rate Oscillations During the Electrochemical Anodization of Cu in Phosphoric Solutions. Some Preliminary Results. *Surf. Sci.* **1987**, *191*, 225.
- Albahadily, F.; Schell, M. *J. Chem. Phys.* **1988**, *88*, 4312.
- Albahadily, F. N.; Ringland, J.; Schell, M. *J. Chem. Phys.* **1989**, *90*, 813.
- Packard, N. H.; Crutchfield, J. P.; Farmer, J. D.; Shaw, R. S. Geometry from a time series. *Phys. Rev. Lett.* **1980**, *45* (9), 712–716.
- Crutchfield, J. P.; McNamara, B. S. Equations of motion from a data series. *Complex Syst.* **1987**, *1*, 417–452.
- Farmer, J. D.; Sidorowitch, J. J. *Phys. Rev. Lett.* **1987**, *59*, 845.
- Agarwal, A. K.; Ahalpara, D. P.; Kaw, P. K.; Prablakera, H. R.; Sen, A. Model Equations from a chaotic time series. *J. Phys.* **1990**, *35* (3), 287–301.
- Breeden, J. L.; Hübler, A. Reconstructing Equations of motion from Experimental Data with Hidden Variables. *Phys. Rev. A* **1990**, *42* (10), 5817–5826.
- Casdagli, M.; Eubank, S.; Farmer, J. D.; Gibson, J. State Space Reconstruction with Noise. *Physica D* **1991**, *51*, 52–98.
- Giona, M.; Lendini, F.; Cimagalli, V. *Phys. Rev. A* **1991**, *44*, 3496.
- Gouesbet, G. Reconstruction of the vector fields of continuous dynamical systems from numerical scalar time series. *Phys. Rev. A* **1991**, *43* (10), 5321–5331.
- Gouesbet, G. Reconstruction of Standard and Inverse Vector Fields Equivalent to a Rössler system. *Phys. Rev. A* **1991**, *44* (10), 6264–6280.
- Palus, M.; Dvorák, I. Singular-value Decomposition in Attractor Reconstruction. Pitfalls and Precautions. *Physica D* **1992**, *55*, 221–234.
- Gouesbet, G. Reconstruction of Vector Fields: the Case of Lorenz System. *Phys. Rev. A* **1992**, *46* (4), 1784–1796.
- Gouesbet, G.; Maquet, J. Construction of phenomenological models from numerical scalar time series. *Physica D* **1992**, *58*, 202–215.
- Gouesbet, G.; Letellier, C. Global vector field reconstruction by using a multivariate polynomial L_2 -approximation on nets. *Phys. Rev. E* **1994**, *49* (6), 4955–4972.
- Letellier, C.; Gouesbet, G. Equivalences between original and reconstructed strange attractors in the case of 3D differential embeddings. Submitted to *Chaos*.
- Gibson, J. F.; Farmer, J. D.; Casdagli, M.; Eubank, S. An Analytic Approach to Practical State Space Reconstruction. *Physica D* **1992**, *57*, 1–30.
- Brown, R.; Rulkov, N. F.; Tracy, E. R. Modelling time series data and synchronizing chaotic systems. *Preprint*, 1993.
- Mindlin, G. B.; Hou, X. J.; Solari, H. G.; Gilmore, R.; Tuffillaro, N. B. Classification of Strange Attractors by Integers. *Phys. Rev. Lett.* **1990**, *64* (20), 2350–2353.
- Tuffillaro, N. B.; Abbott, T.; Reilly, J. *An Experimental Approach to Nonlinear Dynamics and Chaos*; Addison-Wesley: New York, 1992.
- Rössler, O. E. An equation for Continuous Chaos. *Phys. Lett.* **1976**, *57A* (5), 397–398.
- Birman, J. S.; Williams, R. F. Knotted periodic orbits in dynamical systems: Lorenz's equations. *Topology* **1983**, *22* (1), 47–82.
- Melvin, P.; Tuffillaro, N. B. Templates and Framed Braids. *Phys. Rev. A* **1991**, *44* (6), 3419–3422.
- Letellier, C.; Dutertre, P.; Maheu, B. Unstable periodic orbits and templates of the Rössler system: toward a systematic topological characterization. *Chaos* **1994**, *4* (4).
- Collet, P.; Eckmann, J. P. Iterated maps on the interval as dynamical systems. *Progress in Physics*; Jaffe, A., Ruelle, D., Eds.; Birkhäuser: Boston, 1980.
- Hall, T. The creation of Horseshoes. *Nonlinearity* **1994**, *7* (3), 861–924.
- Tuffillaro, N. B.; Wyckoff, P.; Brown, R.; Schreiber, T.; Molteno, T. *Topological time series analysis of a string experiment and its synchronized model*. Preprint, July 31, 1994.
- Fang, H. P. Dynamics of strongly dissipative systems. *Phys. Rev. E* **1994**, *49* (6), 5025–5031.
- Le Sceller, L.; Letellier, C.; Gouesbet, G. Algebraic evaluation of linking numbers of unstable periodic orbits in chaotic attractor. *Phys. Rev. E* **1994**, *49* (5), 4693–4695.
- Mindlin, G. B.; Solari, H. G.; Natiello, M. A.; Gilmore, R.; Hou, X. J. Topological Analysis of Chaotic Time Series Data from the Belousov-Zhabotinski. *J. Nonlinear Sci.* **1991**, *1*, 147–173.
- Couillet, P.; Tresser, C. Itérations d'endomorphismes et groupe de renormalisation. *J. Phys.* **1978**, *8* (39), C5–25. Colloque C5, supplément.
- Feigenbaum, M. J. Quantitative Universality for a Class of Nonlinear Transformation. *J. of Stat. Phys.* **1978**, *19* (1), 25–52.
- Fei, Z.; Hudson, J. L.; Kelly, R. G. *J. Electrochem. Soc.* **1994**, *141* (9), L123.
- Grassberger, P.; Proccacia, I. Measuring the Strangeness of Strange Attractors. *Physica D* **1983**, *9*, 189.
- Crutchfield, J. P.; Farmer, J. D. Fluctuations and simple chaotic dynamics. *Phys. Rep.* **1982**, *92* (2), 45–82.
- Ott, E. *Chaos in dynamical system*; Cambridge University Press: Cambridge, 1993.
- Letellier, C. Caractérisation topologique et reconstruction d'attracteurs étranges. Ph.D. Thesis, LESP, Rouen, 1994.
- Kostelich, E. J.; Yorke, J. A. Noise Reduction: Finding the Simplest Dynamical System Consistent with the Data. *Physica D* **1990**, *41*, 183–196.
- Lapedes, A. S.; Farber, R. F. Nonlinear Signal Processing Using Neural Networks: Prediction and System Modeling. *Los Alamos Report*, LA-UR 87-2882, 1987.
- Casdagli, M. Nonlinear Prediction of Chaotic Time Series. *Physica D* **1989**, *35*, 335–356.